FtsEX-mediated regulation of inner membrane fusion and cell separation reveals morphogenetic plasticity in *Caulobacter crescentus*

Short title:

Cell division mutant reveals plasticity in bacterial morphogenetic programs

Elizabeth L. Meier[1], Qing Yao[2], Allison K. Daitch[1], Grant J. Jensen[2,3] and Erin D. Goley[1#]

[1]Department of Biological Chemistry, Johns Hopkins University School of Medicine, Baltimore, Maryland 21205, USA

[2]Division of Biology and Biological Engineering and [3]Howard Hughes Medical Institute, California Institute of Technology, Pasadena, California 91125, USA

[#]Correspondence and requests for materials should be addressed to E.D.G. (email: egoley1@jhmi.edu).

Abstract

During its life cycle, *Caulobacter crescentus* undergoes a series of coordinated shape changes, including generation of a polar stalk and reshaping of the cell envelope to produce new daughter cells through the process of cytokinesis. The mechanisms by which these morphogenetic processes are coordinated in time and space remain largely unknown. Here we demonstrate that the conserved division complex FtsEX controls both the early and late stages of cytokinesis in *C. crescentus*, namely initiation of constriction and final cell separation. Δ*ftsE* cells display a striking phenotype: cells are chained, with skinny connections between cell bodies resulting from defects in inner membrane fusion and cell separation. Surprisingly, the thin connections in Δ*ftsE* cells share morphological and molecular features with *C. crescentus* stalks. Our data uncover unanticipated morphogenetic plasticity in *C. crescentus*, with loss of FtsE causing a stalk-like program to take over at failed division sites and yield novel cell morphology.

47 **Author Summary**

48 Bacterial cell shape is genetically hardwired and is critical for fitness and, in certain
49 cases, pathogenesis. In most bacteria, a semi-rigid structure called the cell wall surrounds
50 the inner membrane, offering protection against cell lysis while simultaneously
51 maintaining cell shape. A highly dynamic macromolecular structure, the cell wall
52 undergoes extensive remodeling as bacterial cells grow and divide. We demonstrate that
53 a broadly conserved cell division complex, FtsEX, relays signals from the cytoplasm to
54 the cell wall to regulate key developmental shape changes in the α-proteobacterium
55 *Caulobacter crescentus*. Consistent with studies in diverse bacteria, we observe strong
56 synthetic interactions between *ftsE* and cell wall hydrolytic factors, suggesting that
57 regulation of cell wall remodeling is a conserved function of FtsEX. Loss of FtsE causes
58 morphological defects associated with both the early and late stages of division.
59 Intriguingly, without FtsE, cells frequently fail to separate and instead elaborate a thin,
60 tubular structure between cell bodies, a growth mode observed in other α-proteobacteria.
61 Overall, our results highlight the plasticity of bacterial cell shape and demonstrate how
62 altering the activity of one morphogenetic program can produce diverse morphologies
63 resembling those of other bacteria in nature.

64

65

66

67

68

69

Introduction

Bacteria are capable of adopting an impressive array of shapes exquisitely tuned for their particular environmental niches. Underpinning these shapes is the bacterial cell wall, which plays an essential role in specifying and maintaining diverse morphologies [1]. The cell wall consists of a layer of peptidoglycan (PG) composed of glycan strands of repeating disaccharide subunits crosslinked by pentapeptide bridges. In addition to adapting to changing environments, the PG also undergoes dynamic remodeling to drive shape changes during dedicated cellular processes such as division [2,3].

The α-proteobacterium *Caulobacter crescentus* is an ideal model organism for the study of cell shape as it undergoes a series of coordinated morphogenetic changes during its cell cycle. After every division event, *C. crescentus* produces two distinct daughter cell types. One is a flagellated, motile swarmer cell, which contains a flagellum and pili at one cell pole [4]. The other is a sessile stalked cell, where the polar flagellum has been replaced by a thin, tubular extension of the cell envelope known as a stalk [4]. Unable to replicate its chromosome or initiate cell division, a swarmer cell differentiates into a stalked cell by ejecting its flagellum, disassembling its pili, and growing a stalk at the same pole [4]. A stalked cell then elongates its cell body, replicates and segregates its DNA, and produces a flagellum at the pole opposite its stalk prior to cytokinesis. The asymmetric polarization of distinct organelles imparts *C. crescentus* with a highly tractable dimorphic life cycle ideally suited for studying developmental shape changes.

92 One cell cycle event that requires obvious reshaping of the cell envelope is cell division,
93 which, in nearly all bacteria, requires the conserved tubulin homolog FtsZ. A GTPase,
94 FtsZ polymerizes into a patchy annular structure (the Z-ring) at the incipient division site
95 and recruits the downstream division machinery or divisome. Together, FtsZ and
96 proteins of the divisome coordinate invagination and fission of the membrane(s) with
97 extensive cell wall remodeling [5]. A number of division proteins are known to interact
98 directly with FtsZ. For many of these regulators, however, their mechanism of action
99 toward FtsZ and physiological role in division remain to be discovered. One division
100 complex that has been particularly enigmatic is the ATP-binding cassette (ABC)
101 transporter family complex FtsEX, which is widely conserved in bacteria and functions
102 as a heterodimer with FtsE in the cytoplasm and FtsX in the inner membrane. In
103 *Escherichia coli*, FtsEX localizes to the septum and contributes to the efficiency of cell
104 division, particularly in salt-free media [6]. There is no evidence that FtsEX acts as a
105 transporter, however, and recent studies from a wide range of bacteria have instead
106 implicated FtsEX in the activation of cell wall hydrolysis [7-11]. Septal PG material
107 needs to be split to allow for outer membrane constriction and ultimately for separation of
108 the two new daughter cells. In high salt media, *E. coli* Δ*ftsEX* cells exhibit a phenotype
109 similar to cell wall hydrolysis mutants, i.e. cells are chained and mildly filamentous,
110 suggesting a common genetic pathway [9].
111
112 In addition to its involvement in cell wall hydrolysis, in *E. coli*, FtsEX is important for
113 the recruitment of late division proteins and the assembly and/or stability of the septal
114 ring [6]. Interestingly, *E. coli ftsE* mutants impaired for ATP binding and hydrolysis

support Z-ring assembly, but constrict poorly [12]. Since FtsE interacts with FtsZ in *E. coli*, one possibility is that FtsEX functions as a membrane anchor for FtsZ and utilizes ATP binding and hydrolysis to regulate Z-ring constriction [13,6].

In this study, we were originally motivated to characterize FtsEX as a novel membrane anchor for FtsZ in *C. crescentus* since FtsE is one of the first proteins recruited to the nascent division site and is important for efficient cell separation and Z-ring assembly and/or stability [14,15]. Considering the conserved function of FtsEX as a modulator of cell wall remodeling, we asked whether FtsEX, in addition to promoting Z-ring structure, regulates cell wall cleavage in *C. crescentus*. We find that *ftsE* has strong synthetic cell separation defects with cell wall hydrolytic factors. Interestingly, however, deleting *ftsE* produces chains of cell bodies connected by thin, tube-like connections that contain all layers of the cell envelope. This is in stark contrast to the thick, uncleaved septa and compartmentalized cytoplasms observed in hydrolysis mutants from *E. coli* and other organisms. The cell-cell connections of Δ*ftsE* cells are, instead, morphologically and topologically similar to *C. crescentus* stalks. In accordance with their shared morphological features, the stalk proteins StpX and PbpC localize to both the skinny connections and stalks of Δ*ftsE* cells, indicating that stalk formation may be mechanistically similar to the elaboration of the extended constriction sites. Our data reveal unanticipated morphogenetic plasticity in *C. crescentus*, with a stalk-like program taking over at failed division sites in the Δ*ftsE* mutant to yield novel cell morphology.

Results

Δ*ftsE* cells form chains connected by skinny constrictions

To begin to address the role of FtsEX in *C. crescentus*, we first attempted to make *ftsE* and *ftsX* deletion strains. Although *ftsE* is annotated as essential [16,14], we successfully made several independent Δ*ftsE* clones [15]. *ftsX* is also annotated as essential [16], but unlike *ftsE*, we were unable to make an *ftsX* deletion, depletion, or overexpression strain, suggesting that *C. crescentus* cells are highly sensitive to changes in FtsX levels. To understand the role of the FtsEX complex in *C. crescentus* morphogenesis, we focused on characterizing the *ftsE* mutant in detail. Δ*ftsE* cells displayed a striking division phenotype consisting of chained cells with skinny, extended connections between cell bodies. Consistent with the chaining phenotype, Δ*ftsE* cells are longer and grow more slowly than WT [15]. Transmission electron microscopy (TEM) offered us better resolution of cells lacking FtsE (Fig 1). Δ*ftsE* cell bodies were heterogeneous in length, but overall appeared elongated compared to WT, which suggests a delay or inefficiency in the initiation of constriction. The thin connections between Δ*ftsE* cell bodies were also heterogeneous in length, with some extending hundreds of nanometers, and had dimensions qualitatively similar to those observed for stalks (Fig 1B). Overall, the Δ*ftsE* phenotype supports a role for FtsE both in the initiation of constriction and in late stage cell separation.

FtsE promotes focused Z-ring organization

FtsE has been reported to bind FtsZ in *E. coli*, is one of the first division proteins to localize to midcell after FtsZ in *C. crescentus*, and *C. crescentus* Δ*ftsE* cells have aberrant

Z-rings [13-15]. Specifically, in Δ*ftsE* cells FtsZ is more diffuse and often localizes as clusters of puncta instead of focused Z-rings (Fig 2) [15]. These data suggest that FtsE may regulate early Z-ring structure and/or assembly. Consequently, we tested if *ftsE* interacted genetically with the positive Z-ring regulator *zapA*, which, like FtsE, is also recruited early to midcell by FtsZ in *C. crescentus* [17,14]. Δ*zapA*Δ*ftsE* cells displayed mild synthetic growth and cell length defects, but had severely disrupted, diffuse Z-ring structures (Fig 2). We also observed that Δ*zapA*Δ*ftsE* cells were very sensitive to even slight increases in FtsZ levels and were noticeably filamentous after only one hour of *ftsZ-cfp* expression (Fig 2D). We conclude that FtsE contributes to proper Z-ring focusing at midcell and that the elongated cell bodies in Δ*ftsE* are likely due to inefficient initiation of constriction by the aberrant FtsZ structures.

Excess FtsE or FtsEX alters the localization of FtsZ and new cell wall synthesis

Because cells lacking FtsE have perturbed Z-ring organization, we hypothesized that overproducing FtsE would affect Z-ring structure, particularly if FtsE binds directly to FtsZ. Overexpression of either *ftsE* or *ftsEX* caused dramatic filamentation, and overexpression of *ftsE* alone also caused ectopic poles to form (Fig 3). After four hours of FtsE overproduction, instead of Z-rings, FtsZ-CFP formed discrete puncta along the length of the filamentous cells (Fig 3A). Interestingly, when we overproduced FtsEX, FtsZ-CFP localized in a drastically different pattern, as multiple wide bands (Fig 3A). *C. crescentus* Z-ring positioning is in part dictated by a negative regulator of FtsZ assembly called MipZ, which forms a complex near the origin of replication [18]. After the polar origin region is duplicated, the second copy is quickly transported to the opposite cell

pole. Bipolar MipZ thereby directs Z-ring assembly at midcell by inhibiting FtsZ polymerization at the poles [18]. MipZ-YFP localized at the poles and as fairly regularly spaced puncta in cells overproducing FtsE or FtsEX, but its localization was more diffuse in cells overproducing FtsEX (Fig 3B). We interpret the MipZ localization data as evidence that chromosomal replication and segregation still occur in cells overproducing FtsE despite the inhibition of division; however high levels of FtsEX may interfere with levels or localization of MipZ.

In *C. crescentus*, FtsZ directs new cell wall synthesis at midcell even before the onset of division (Fig 3C) [19]. To determine if the FtsZ structures in FtsE or FtsEX overproducing cells were competent to localize new cell wall synthesis, we pulse-labeled cells with the fluorescent D-amino acid hydroxycoumarin-carbonyl-amino-D-alanine (HADA), which can replace D-Ala^4 or D-Ala/Gly^5 in the lipid II peptide side chain, to track the incorporation of newly synthesized PG [20]. High levels of FtsE resulted in diffuse HADA labeling which closely resembled the pattern of HADA incorporation in FtsZ-depleted cells (Fig 3C). This result suggests that the FtsZ puncta associated with *ftsE* overexpression are unable to direct local cell wall metabolism. Cells overexpressing *ftsEX*, however, had discrete, wide bands of new PG incorporation, likely directed by the similarly organized Z-ring structures (Fig 3C). Thus, high levels of FtsE or FtsEX not only differentially affect Z-ring organization, but also affect FtsZ's ability to locally incorporate new cell wall material at midcell. Specifically, the intact FtsEX complex is required both for formation of Z-rings and downstream communication with PG synthetic machinery.

207

208 **_ftsE_ interacts genetically with PG hydrolytic factors and a regulator of stalked pole**
209 **development**

210 Since FtsEX has been implicated in cell wall hydrolysis in numerous bacteria and Δ*ftsE*
211 cells displayed a cell chaining phenotype, we asked whether FtsEX, in addition to
212 promoting Z-ring structure, regulates *C. crescentus* cell wall hydrolysis. In *E. coli*,
213 periplasmic *N*-acetylmuramyl-$_L$-alanine amidases AmiA/B/C are responsible for cleaving
214 bonds that link stem peptides to glycan strands at the septum [21]. The amidases require
215 activation by the LytM domain containing proteins EnvC, which stimulates AmiA/B, and
216 NlpD, which stimulates AmiC, to split apart septal PG [22,23]. FtsEX directly recruits
217 EnvC to the septum via the periplasmic extracellular loop (ECL) of FtsX and the coiled
218 coil (CC) domain of EnvC [9]. *C. crescentus* possesses a limited number of lytic
219 enzymes involved in peptidoglycan remodeling, with only a single *N*-acetylmuramyl-$_L$-
220 alanine amidase, most similar to *E. coli* AmiC [24,25]. There are at least seven genes
221 coding for putative LytM domain containing proteins; however, the only characterized
222 protein in the *C. crescentus* LytM family is DipM, which participates in cell wall
223 remodeling and coordinated constriction of the cell envelope layers at the division plane
224 [25-27]. To determine whether the FtsEX PG hydrolysis paradigm applies to *C.*
225 *crescentus*, we performed a BLAST search for *E. coli* EnvC homologues and found
226 CCNA_03547, which we will hereafter refer to as *L*ytM *d*omain *p*rotein *F* (LdpF)
227 (Martin Thanbichler, personal communication). Like EnvC, LdpF is a LytM domain
228 containing protein with a signal peptide, two N-terminal CC domains, and a C-terminal

LytM domain (Fig S1A). We hypothesized that *C. crescentus* FtsEX-LdpF-AmiC may function in an activation pathway analogous to *E. coli* FtsEX-EnvC-AmiA/B.

We first adopted a genetic approach to investigate the role of FtsEX in cell wall hydrolysis during division. In *E. coli*, FtsEX is required for EnvC's localization at midcell [9]. However, LdpF-mCherry is diffuse, and we did not observe differences in its localization between WT and Δ*ftsE* cells (Fig S1B). Although *E. coli* cells lacking EnvC or AmiA/B are not as sick as cells lacking FtsEX, part of the division defect associated with loss of FtsEX may be due to EnvC inactivation [9]. Consistent with this reasoning, in *C. crescentus*, cells lacking LdpF or AmiC had mild chaining and growth defects compared to Δ*ftsE* cells (Fig 4). Depleting AmiC in Δ*ftsE* or Δ*ldpF* backgrounds caused strong synthetic cell separation and growth defects, accompanied by noticeable lengthening of the skinny connections between cell bodies, particularly in the *ftsE* mutant (Fig 4). Combining Δ*ldpF* with loss of FtsE produced only mild synthetic growth and chaining defects, which is consistent with them acting in a common pathway (Fig 4).

E. coli cells lacking EnvC depend on NlpD for cell separation: simultaneous inactivation of either EnvC or FtsEX and NlpD results in severe chaining, supporting the hypothesis that FtsEX activates EnvC's ability to promote septal PG cleavage [22]. In *C. crescentus*, the LytM protein most closely related to NlpD is DipM, which has similar domain organization to NlpD but differs in that it is not associated with the outer membrane. Depleting AmiC in cells lacking DipM caused a moderate synthetic growth defect, whereas depletion of DipM in Δ*ftsE* or Δ*ldpF* cells was synthetic lethal (Fig 5). The

252 synthetic defects associated with loss of DipM with FtsE, LdpF, or AmiC as well as the
253 distinct morphology of Δ*dipM* cells [25-27] suggests that DipM operates in a non-
254 redundant, parallel hydrolytic pathway. We also hypothesize, based on the strong
255 synthetic interactions between AmiC and FtsE or LdpF but only mild synthetic defects
256 associated with loss of FtsE and LdpF, that AmiC operates in a hydrolytic pathway
257 separate from FtsE and LdpF. However, it is apparent that all three putative PG
258 hydrolytic pathways contribute to the efficiency of cell separation in *C. crescentus*.
259
260 Interestingly, in a transposon deep-sequencing analysis to uncover transposon insertions
261 that alter the competitive fitness of Δ*spmX* cells, the *ftsE* and *ldpF* loci were the first and
262 second least favored insertion sites, respectively, in Δ*spmX* cells as compared to WT [28].
263 We therefore tested for synthetic interactions between *ftsE* and *spmX*, which encodes a
264 muramidase homolog that localizes to the stalked cell pole and controls the swarmer-to-
265 stalk cell transition [29]. Consistent with the Δ*spmX* transposon deep-sequencing results,
266 we observed severe synthetic growth and morphological defects for Δ*ftsE*Δ*spmX* cells,
267 implicating FtsE and LdpF in the stalked pole development pathway, likely through a
268 connection to cell wall remodeling (Fig 5E).
269
270 **The CC domain of LdpF interacts with the ECL of FtsX, but LdpF does not activate**
271 **AmiC PG hydrolysis *in vitro***
272 To provide biochemical support for our *in vivo* findings, we purified LdpF, AmiC, DipM,
273 and the ECL of FtsX, and monitored PG degradation using an *in vitro* dye release assay
274 [30,23]. Although bacterial two hybrid showed a positive interaction for the ECL of FtsX

and the CC domain of LdpF, we did not observe LdpF-activated AmiC PG hydrolysis *in vitro* (Fig S2; S1 Text). Interestingly, the LytM domain of DipM was sufficient to mildly stimulate AmiC hydrolase activity *in vitro* (Fig S2C; S1 Text). However, as *C. crescentus* DipM and AmiC are most similar to the *E. coli* activator-amidase pair, NlpD and AmiC, perhaps this result is unsurprising. In light of the distinct phenotypes of cells lacking DipM and AmiC, however, we suspect that DipM has activities in addition to the regulation of AmiC. Collectively, our genetic and biochemical evidence indicate at least three hydrolytic pathways in *C. crescentus* and implicate a yet unidentified downstream target of FtsEX-LdpF in the regulation of PG metabolism.

Electron cryotomography reveals unique cell envelope organization at chaining sites

Our genetic evidence is consistent with a role for FtsEX in regulating cell wall hydrolysis for cell separation. Although TEM highlighted the general cell separation defects of Δ*ftsE* cells (Fig 1), electron cryotomography (ECT) allowed us to dissect the exact stages at which these cells are blocked during division (Fig 6). To capture the cell envelope organization at the skinny cell-cell connections, we imaged cells lacking both FtsE and AmiC since loss of AmiC exacerbates the Δ*ftsE* chaining phenotype (Fig 4). In five out of six tomograms, we could identify with certainty the presence of all layers of the cell envelope in the skinny connections between chained cell bodies (Fig 6). Four of these had obvious cytoplasmic volume between the unfused inner membranes. In at least one example, however, the inner membranes were closely stacked on top of each other, but not fused (Fig 6).

In WT *C. crescentus*, the final stages of inner membrane fission are rapid, and the smallest diameter for inner membrane connections that have been captured by ECT are ~60 nm [31]. In cells lacking FtsE and AmiC with fairly uniform connections (Fig 6B, D), we observed inner membrane diameters ranging from ~12 to 60 nm. Others were more variable and had intermittent bulging, with inner membrane diameters ranging from ~20 to 300 nm within a single cell-cell connection (Figs 6C, S3). This organization of the cell envelope is strikingly different from other mutants deficient in cell wall hydrolysis. *E. coli* cells lacking EnvC and NlpD or all four LytM-domain containing factors complete inner membrane fusion and cytoplasmic compartmentalization, but struggle to constrict their outer membrane due to a layer of intact PG between adjacent chained cells [22]. Similarly, Δ*dipM* cells form chains with fused inner membranes and thick, multilayered PG between cell bodies [25,26]. Therefore, the cell envelope organization of cells lacking FtsE and AmiC, namely the continuous cytoplasmic connections and narrow spacing between the inner membranes, represents a unique cell separation phenotype and, potentially, a novel pathway for cell separation in *C. crescentus.*

Δ*ftsE* thin connections are morphologically stalk-like and enriched for stalk proteins

During its dimorphic life cycle, *C. crescentus* elaborates a polar stalk, a tubular extension of the cell envelope important for nutrient uptake [32]. ECT of cells lacking FtsE and AmiC reinforced an observation we had previously made based on TEM of Δ*ftsE*, namely, the striking morphological similarities between the extended connections of *ftsE* mutants and *C. crescentus* stalks (Figs 1, 6). In addition to sharing approximate widths (~12-300 nm inner membrane diameter for the skinny connections; ~20-40 nm inner

membrane diameter for the stalks) and cell envelope organization, we occasionally observed electron dense structures that spanned the short axis of the cell envelope of the thin connections (Fig 6). These structures were reminiscent of stalk cross-bands, multiprotein assemblies that transect the stalk at regular intervals and function as diffusion barriers to compartmentalize stalk and cell body periplasmic and membrane proteins (Figs 6A,C, D, S3) [33].

Since stalk growth occurs by incorporation of new material at the cell body-stalk junction [32], we monitored HADA incorporation at the extended constrictions of *ftsE* mutants. In general, we observed incorporation of new cell wall material throughout the skinny connections (Fig S4), which contrasts with the pattern of *de novo* PG synthesis only at the base of stalks. There are two modes of zonal PG synthesis in *C. crescentus*: FtsZ-independent PG incorporation at the base of the stalk and FtsZ-dependent PG incorporation at midcell [19]. Interestingly, in Δ*ftsE* cells, FtsZ is not enriched at the skinny connections suggesting that the new cell wall synthesis occurring throughout the skinny connections is an FtsZ-independent process similar to PG synthesis at the base of the stalk (Fig S4).

Motivated by the morphological similarities between the extended constrictions in Δ*ftsE* cells and *C. crescentus* stalks, we asked if any stalk-specific proteins could localize to the skinny connections. StpX is a bitopic membrane protein enriched in the stalk that regulates stalk length [34]. We expressed *stpX-cfp* in WT, Δ*ftsE*, and Δ*ftsE* cells lacking AmiC: StpX-CFP localized to the stalks in all genetic backgrounds, but strikingly, was

344 also enriched at the skinny constrictions in the *ftsE* mutant cells (Fig 7A). The
345 bifunctional penicillin binding protein, PbpC, is involved in stalk elongation [35] and is
346 required to sequester StpX at the stalk in WT *C. crescentus* [37]. To investigate the
347 localization dependency of StpX to the skinny constrictions, we expressed *stpX-cfp* in a
348 Δ*ftsE*Δ*pbpC* mutant background. Consistent with previous reports, StpX-CFP was not
349 enriched in stalks in cells lacking both FtsE and PbpC. However, StpX-CFP was also not
350 enriched at the skinny connections between cells and instead was diffusely localized at
351 the cell periphery (Fig 7B). We also expressed *pbpC-yfp* in WT and Δ*ftsE* cells and
352 observed enrichment at the base of stalks as well as frequent localization to the skinny
353 connections in the *ftsE* mutant (Fig 7C). Since we observe enrichment of both PbpC and
354 StpX at the skinny connections in Δ*ftsE* cells, we hypothesize that PbpC initially recruits
355 StpX to the skinny connections and promotes its retention at those sites.
356
357 Considering the presence of both PbpC and StpX at the skinny connections in the *ftsE*
358 mutant, we monitored the localization of the stalk cross-band protein, StpB. StpB-
359 mCherry localized as puncta in the stalks of WT, Δ*ftsE*, and Δ*ftsE* cells lacking AmiC,
360 but was not enriched at the extended constriction sites (Fig. 7D). Consequently, the
361 proteinaceous, envelope-spanning discs observed in the *ftsE* mutant by ECT (Fig 6) may
362 not, in fact, be cross-bands or may differ in molecular composition from stalk cross-
363 bands. We conclude that the skinny connections share numerous morphological and
364 molecular similarities with stalks, but the two structures are not physically or
365 biochemically identical.
366

Discussion

The role of FtsEX in synchronizing PG remodeling with cell division appears to be conserved amongst distantly related bacterial species such as *E. coli*, *S. pneumoniae*, and *M. tuberculosis*, although the downstream adaptor or enzyme targets vary [7-11]. We provide evidence that this paradigm also extends to the α-proteobacterium *C. crescentus*. Our data indicate that FtsE is important for initial Z-ring assembly and regulates Z-ring structure in a manner dependent on its stoichiometry with FtsX (Figs 2, 3, 8A). Different levels of FtsE or FtsEX not only affect FtsZ localization, but also FtsZ function, namely its ability to localize incorporation of new cell wall material (Fig 3). Additionally, our data implicate FtsEX in a cell wall metabolic pathway involving LdpF and an unidentified downstream cell wall factor regulated by LdpF (Fig 4, 8B). Thus *C. crescentus* FtsEX, similar to what has been proposed in *E. coli*, may synchronize PG remodeling with Z-ring constriction during division [9]. ECT of the skinny connections in Δ*ftsE* revealed a cell envelope architecture remarkably distinct from *E. coli* hydrolase mutants, however, and an overall morphology that was strikingly stalk-like (Fig 6). Enrichment for stalk proteins StpX and PbpC at the skinny constrictions in Δ*ftsE* and a strong genetic interaction between *ftsE* and the stalked cell fate determinant *spmX* further support mechanistic overlap between the elaboration of thin connections in *ftsE* mutants and stalk development (Figs 5, 7, 8A).

During the late stages of division in *C. crescentus*, constriction of the inner membrane proceeds until the inner membranes of the two future daughter cell compartments are connected only by a small tubular structure [31]. Out of thousands of cells Judd and

colleagues examined in their study, only five displayed inner membranes with diameters less than ~100 nm and the smallest inner membrane connection was 60 nm in diameter [31]. ECT of cells lacking FtsE and AmiC with fairly uniform connections showed inner membrane diameters ranging from ~12 to 60 nm (Fig 6). Thus, the majority of cells lacking FtsE and AmiC have inner membrane diameters that fall well below the lowest threshold reported for inner membrane diameters at any stage of WT cell division. Furthermore, WT cells spend a short amount of time in these late, transitional stages, perhaps only a few seconds, and membrane topology changes very rapidly [31]. In the case of *ftsE* mutant cells, the thin connections are abundant in a mixed cell population and, based on their nearly abutting inner membranes, are likely blocked or delayed at a terminal stage just prior to inner membrane fission. In WT *C. crescentus*, the mechanisms underlying rapid terminal constriction and membrane fusion are unknown [31]. Our data indicate that FtsEX is important for inner membrane fusion, either directly or indirectly, and that in the absence of FtsE, inner membrane fusion frequently fails, PG synthesis continues, and cells elaborate a stalk-like structure.

Understanding how proteins are targeted specifically to the stalk is important for understanding mechanisms of subcellular organization in bacteria as well as stalk function [36]. We have limited knowledge about the molecular pathways responsible for targeting proteins to the stalk; however, stalked pole geometry, membrane curvature, or unique peptidoglycan motifs are possible mechanisms for protein localization at the stalk. The observation that both StpX and PbpC localize to the skinny connections in Δ*ftsE* cells provides an experimental handle for understanding stalk biogenesis and stalk protein

413 localization cues. In WT *C. crescentus*, the bactofilins, BacA and BacB, localize at the
414 stalked pole and recruit PbpC during the swarmer-to-stalked cell transition [35]. We
415 have not monitored the localization of the bactofilins in Δ*ftsE* cells, but we predict that
416 they would localize at the skinny connections upstream of PbpC, similar to the protein
417 recruitment hierarchy observed for stalks. It has been proposed that the membrane
418 curvature at the stalk-cell body junction drives BacAB clusters to localize there [35].
419 These BacAB clusters could likewise recruit PbpC and StpX to the junctions between the
420 cell bodies and skinny connections in Δ*ftsE* on the basis of shared membrane curvature
421 with the cell body-stalk junction. Additionally, the composition of the peptidoglycan is
422 purportedly distinct between the cell body and the stalk [37], as stalks are more resistant
423 to lysozyme treatment [38]. PbpC may regulate the rigidity of the stalk by dictating a
424 specific cell wall remodeling regime, which may also be active at the skinny connections
425 [35]. The periplasmic N-terminal domain of StpX is required for its stalk localization
426 and may recognize PbpC-specific changes in PG chemistry, leading to sequestration of
427 StpX in the stalk and the skinny constrictions of Δ*ftsE* cells [34].
428
429 Within α-proteobacteria, asymmetric patterns of growth are particularly well-represented
430 in the orders *Rhizobiales* and *Caulobacterales* [39]. Unlike *C. crescentus*, which divides
431 by asymmetric binary fission, *Rhodomicrobium vannelliei* and *Hyphomonas neptunium*,
432 members of *Rhizobiales* and *Caulobacterales* respectively, use a budding mechanism
433 whereby new offspring emerges from the tip of a stalk structure [40,39]. Cell division
434 thus occurs in an extremely asymmetric manner at the bud neck, producing a stalked
435 mother cell and a non-stalked daughter cell [39]. After initially increasing in cell size by

436 dispersed PG incorporation, *H. neptunium* displays a period of zonal growth at the new
437 cell pole leading to the elaboration of a stalk structure [39]. This type of stalk outgrowth
438 is similar to what occurs in other stalked α-proteobacteria like *C. crescentus*, which
439 suggests conservation of core machinery. The asymmetric manner in which *H.*
440 *neptunium* divides exemplifies how stalks may function not only as specialized
441 organelles, but also as division planes, depending on the bacterial species [39]. The
442 morphology of Δ*ftsE* cells, with thin, stalk-like extensions between cell bodies is
443 reminiscent of a predivisional *H. neptunium* cell where the stalk is closely integrated
444 within the cell division program.
445
446 While specialized protein machineries exist for cell division and cell elongation, there is
447 no single protein, much less entire machinery, absolutely and specifically required for
448 stalk formation. Since the elongation machinery proteins MreB and RodA contribute to
449 stalk growth and morphogenesis, stalk synthesis has been proposed to be a specialized
450 form of cell elongation [41]. Thus, it is possible that the skinny, stalk-like connections
451 between cell bodies in Δ*ftsE* are a result of a modified form of cell elongation, similar to
452 what has been postulated for stalks [41]. Our data suggest that although the slender
453 connections in Δ*ftsE* share certain morphological and molecular features with stalks, they
454 are not, in actuality, ectopic stalks forming at failed division sites: the spatial pattern of
455 PG incorporation is distinct from stalks, the diameters are not as homogeneous as for
456 stalks, and StpB does not localize at the skinny connections (Figs S3, 6, 7). We instead
457 favor the hypothesis that when Δ*ftsE* cells stall at a late stage in division, the division
458 machinery disengages and the cell elongation machinery takes over and elaborates a thin,

459 stalk-like connection. We interpret this phenomenon as an example of morphogenetic
460 plasticity, whereby small changes to established morphogenetic machineries give rise to
461 novel or, in the case of Δ*ftsE*, modified forms of preexisting structures. Overall, our
462 findings have important implications for understanding late stage division regulation,
463 stalk formation, and the coordination of morphogenetic events and machineries in *C.*
464 *crescentus*. Loss of FtsE has revealed unexpected morphogenetic plasticity between the
465 division and stalk synthesis programs and offers insight into the geneses of diverse
466 morphologies in bacteria.
467
468
469
470
471
472
473
474
475
476
477
478
479
480
481

Materials and Methods

Growth conditions for bacterial strains

C. crescentus NA1000 strains were grown in peptone yeast extract (PYE) medium at 30^{o}C [42]. Additives and antibiotics were used at the following concentrations in liquid (solid) media for *C. crescentus*: xylose 0.3 (0.3)%, glucose 0.2 (0.2)%, vanillate 0.5 (0.5) mM, gentamycin 1 (5) μg ml^{-1}, kanamycin 5 (25) μg ml^{-1}, spectinomycin 25 (100) μg ml^{-1}, streptomycin (5 μg ml^{-1}). Before changes in induction conditions, cells were washed two to three times in plain media. Growth rate analyses were performed in 96-well plates with shaking at 30^{o}C using a Tecan Infinite 200 Pro plate reader. Strains and plasmids used in this study are included as Supporting Information Table S1.

Light microscopy and image analysis

Cells were imaged during the log phase of growth after immobilization on 1% agarose pads. Light microscopy was performed on a Nikon Eclipse Ti inverted microscope equipped with a Nikon Plan Fluor x 100 (numeric aperture 1.30) oil Ph3 objective and Photometrics CoolSNAP HQ cooled CCD (charge-coupled device) camera. Chroma filter cubes were used as follows: ET-EYFP for YFP and ET-ECFP for CFP, ET-dsRED for mCherry and ET-ECFP for HADA. Images were processed in Adobe Photoshop. Automated cell length analysis was performed using Oufti or MicrobeTracker [43]. In MicrobeTracker, algorithm 4 was used for determining cell outlines, with the following parameter change: areaMin=150.

505 ***Whole cell TEM***

506 Cells from EG864 and EG1133 were grown in PYE and prepared for whole cell TEM
507 exactly as described [42].

508

509 ***HADA labeling***

510 Cells from strains EG213, EG379, EG864, EG930, EG1133, EG1252, EG1272, and
511 EG1863 were grown in PYE. HADA [20] was added to 0.41 mM and the cultures were
512 returned to the shaker for 5 min. The cells were then washed twice with PBS and
513 resuspended in PBS before imaging [42].

514

515 ***Bacterial two-hybrid***

516 The T18 and T25 plasmids were co-transformed into BTH101 (*F-*, *cya-99*, *araD139*,
517 *galE15*, *galK16*, *rpsL1 (Str^r)*, *hsdR2*, *mcrA1*, *mcrB1*; Euromedex) competent cells,
518 plated onto LB agar with ampicillin (100 µg/µl) and kanamycin (50 µg/µl), and incubated
519 overnight at 30^{o}C. Several colonies were inoculated into LB with ampicillin (100 µg/µl),
520 kanamycin (50 µg/µl), and IPTG (0.5 mM) and incubated at 30^{o}C overnight. The next
521 morning 2 µl of each culture was spotted onto plates containing ampicillin, kanamycin,
522 X-gal (40 µg/ml), and IPTG (0.5 mM) and incubated for 1-2 days at 30^{o}C. Positive
523 interactions were indicated by blue colonies. Every interaction was tested in triplicate.

524

525 ***Electron cryotomography (ECT)***

526 For ECT imaging, strain EG1863 was grown in PYE with xylose. Once in log phase,
527 EG1863 was washed twice with PYE and resuspended in PYE without xylose to deplete

AmiC. EG1863 was then grown in PYE without xylose for ~6 h, transferred to an eppendorf tube, and shipped on ice to Grant Jensen's lab at Caltech. The total amount of time the cells spent on ice was ~24 h. We imaged and monitored CFUs of EG1863 cells before shipment and after 24 h of incubation on ice and observed similar growth and morphology. Upon arrival, 1 ml of the EG1863 culture was centrifuged at 3000 rpm for 5 min and resuspended in fresh PYE to a final OD_{600} of ~8. This resuspension was mixed with fiducial markers (10 nm gold beads treated with bovine serum albumin to prevent aggregation) and 2 µl of the resuspension mixture was plunge-frozen on EM grids in a mixture of liquid ethane and propane [44]. Images were acquired using a 300 keV Polara transmission electron microscope (FEI) equipped with a GIF energy filter (Gatan) and a K2 Summit direct detector (Gatan). Tilt-series were collected from -50° to +50° in 1° increments at magnification of 22,500X using UCSF Tomography software [45] with a defocus of -12 µm and total dosage of 180 $e^-/Å^2$. Tomograms were calculated using IMOD software [46].

Protein purification

Rosetta pLysS *E. coli* cells containing overexpression plasmids for AmiC, LdpF, DipM, and truncated LytM domain protein variants, all with a His_6-SUMO tag fused to the N-terminus, were purified as described previously with minor changes [15]. Rosetta cells containing the constructs were grown in 1 L of LB at 30°C to an OD_{600} of 0.4 and then induced with 1 mM IPTG for 4 h. Cells were collected by centrifugation at 6000 x g at 4°C for 10 minutes and resuspended in 40 ml Column Buffer A (CBA: 50 mM Tris-HCl pH 8.0, 300 mM NaCl, 10% glycerol, 20 mM imidazole) per 1 L of culture. Cells were

551 snap-frozen in liquid nitrogen and stored at -80°C until use. Pellets were thawed at 37°C
552 and lysozyme was added to 1 µg/ml and $MgCl_2$ to 2.5 mM. Cell suspensions were left on
553 ice for 45 minutes, then sonicated and centrifuged for 30 minutes at 15,000 x g at 4°C.
554 The protein supernatant was filtered and loaded onto a HisTrap FF 1ml column (GE Life
555 Sciences) pre-equilibrated with CBA. The protein was eluted with 30% Column Buffer
556 B (same as CBA except with 1M imidazole). The protein fractions were combined and
557 His_6-Ulp1 (SUMO protease) was added (1:500 Ulp1:protein molar ratio). The protease
558 and protein fractions were dialyzed overnight at 4°C into CBA. Cleaved protein was run
559 over the same HisTrap FF 1mL column equilibrated in CBA and the flow-through was
560 collected. Flow-through fractions were dialyzed overnight at 4°C into Storage Buffer (50
561 mM HEPES-NaOH pH 7.2, 150 mM NaCl, 10% glycerol). Dialyzed protein was then
562 concentrated (if needed), snap-frozen in liquid-nitrogen, and stored at -80°C.
563
564 ***RBB labeled sacculi preparation***
565 Sacculi were prepared from strain EG865 as described in [23]. *C. crescentus* cells were
566 grown in 1 L of PYE at 30°C, collected at an OD_{600} of 0.6 by centrifugation at 6,000 x g
567 for 10 minutes, and resuspended in 10 ml of PBS. The cell suspension was added drop
568 wise to 80 ml of boiling 4% sodium dodecyl sulfate (SDS) solution. Cells were boiled
569 and mixed for 30 minutes and then incubated overnight at room temperature. Sacculi
570 were then pelleted by ultra-centrifugation at ~80,000 x g for 60 minutes at 25°C. Pelleted
571 sacculi were then washed four times with ultra-pure water and resuspended in 1 ml of
572 PBS and 20 µl of 10 mg/ml amylase and incubated at 30°C overnight. The next day,
573 sacculi were pelleted at ~400,000 x g for 15 minutes at room temperature, washed three

574 times with ultra-pure water, and resuspended in 1 ml of water. The sacculi suspension
575 was labeled with 0.4 ml of 0.2 M remazol-brilliant blue (RBB), 0.3 ml 5 M NaOH, and
576 4.1 ml of water, and incubated at 30°C overnight. The labeled solution was neutralized
577 with 0.4 ml of 5 M HCl and 0.75 ml of 10X PBS. Labeled sacculi were pelleted at
578 16,000 x g for 20 minutes at room temperature. The pellet was washed with water until
579 the supernatant was clear. Blue-labelled sacculi were resuspended in 1 ml of 0.2% azide,
580 incubated at 65°C for 3 hours, and then stored at 4°C.
581
582 ***Dye-release assay***
583 The dye release assay was adapted from [23]. Briefly, 10 µl of RBB-labeled sacculi was
584 incubated at 30°C for 3 hours with AmiC, LdpF variants, DipM variants, or FtsX ECL
585 singly or in combination. All proteins were used at 4 µM. Total reaction volumes were
586 brought to 100 µl with PBS. Lysozyme (4 µM) was used as a positive control. After 3
587 hours of incubation, reactions were heat inactivated at 95°C for 10 minutes and
588 centrifuged for 20 minutes at 16,000 x g. Supernatants were collected and the absorbance
589 was measured at OD_{595}.
590
591
592
593
594
595
596

Acknowledgements

We thank Jasmine Burrell for her work characterizing stalk protein localization in Δ*ftsE*; Martin Thanbichler for sharing plasmids, strains and preliminary LdpF data; Yves Brun, Erkin Kuru, and Michael van Nieuwehnze for HADA; Yves Brun and Ellen Quardokus for assistance with TEM and for sharing the StpX-GFP plasmid; and Zhuo Li for providing the wild-type stalks images in Fig. S3. This work was supported in part by the National Institutes of Health grants R35 GM122588 (to GJJ) and R01 GM108640 (to EDG).

620

621 **References**

622 1. Jiang C, Caccamo PD, Brun YV. Mechanisms of bacterial morphogenesis:
623 evolutionary biology approaches provide new insights. Bioessays. 2015;37(4):
624 413-25.
625 2. Typas A, Banzhaf M, Gross CA, Vollmer W. From the regulation of
626 peptidoglycan synthesis to bacterial growth and morphology. Nat Rev Microbiol.
627 2011;10(2): 123-36. doi: 10.1038/nrmicro2677.
628 3. Woldemeskel SA and Goley ED. Shapeshifting to survive: shape determination
629 and regulation in Caulobacter crescentus. Trends Microbiol. 2017; doi:
630 http://dx.doi.org/10.1016/j.tim.2017.03.006. In press corrected proof.
631 4. Curtis PD and Brun YV. Getting in the loop: regulation of development in
632 Caulobacter crescentus. Microbiol Mol Biol Rev. 2010;74(1): 13-41.
633 5. Meier EL and Goley ED. Form and function of the bacterial cytokinetic ring. Curr
634 Opin Cell Biol. 2014;26: 19-27. doi: 10.1016/j.ceb.2013.08.006.
635 6. Schmidt KL, Peterson ND, Kustusch RJ, Wissel MC, Graham B, Phillips GJ, et
636 al. A predicted ABC transporter, FtsEX, is needed for cell division in Escherichia
637 coli. J Bacteriol. 2004;186(3): 785-93.
638 7. Sham LT, Barendt SM, Kopecky KE, Winkler ME. Essential PcsB putative
639 peptidoglycan hydrolase interacts with the essential FtsXSpn cell division protein
640 in Streptococcus pneumonaie D39. Proc Natl Acad Sci USA. 2011;108(45):
641 E1061-9. doi: 10.1073/pnas.1108323108.

642 8. Sham LT, Jensen KR, Bruce KE, Winkler ME. Involvement of FtsE ATPase and
643 FtsX extracellular loops 1 and 2 in FtsEX-PcsB complex function in cell division
644 of Streptococcus pneumoniae D39. MBio. 2013;4(4). pii: e00431-13. doi:
645 10.1128/mBio.00431-13.
646 9. Yang DC, Peters NT, Parzych KR, Uehara T, Markovski M, Bernhardt TG. An
647 ATP-binding cassette transporter-like complex governs cell-wall hydrolysis at the
648 bacterial cytokinetic ring. Proc Natl Acad USA. 2011;108(45): E1052-60. doi:
649 10.1073/pnas.1107780108.
650 10. Meisner J, Montero Llopis P, Sham LT, Garner E, Bernhardt TG, Rudner DZ.
651 FtsEX is required for CwlO peptidoglycan hydrolase activity during cell wall
652 elongation in Bacillus subtilis. Mol Microbiol. 2013;89(6): 1069-83. doi:
653 10.1111/mmi.12330.
654 11. Mavrici D, Marakalala MJ, Holton JM, Prigozhin DM, Gee CL, Zhang YJ.
655 Mycobacterium tuberculosis FtsX extracellular domain activates the
656 peptidoglycan hydrolase, RipC. Proc Natl Acad Sci USA. 2014;111(22): 8037-42.
657 doi: 10.1073/pnas.1321812111.
658 12. Arends SJ, Kustusch RJ, Weiss DS. ATP-binding site lesions in FtsE impair cell
659 division. J Bacteriol. 2009;191(12): 3772-84. doi: 10.1128/JB.00179-09.
660 13. Corbin BD, Wang Y, Beuria TK, Margolin W. Interaction between cell division
661 proteins FtsE and FtsZ. J Bacteriol. 2007;189(8): 3026-35.
662 14. Goley ED, Yeh YC, Hong SH, Fero MJ, Abeliuk E, McAdams HH, et al.
663 Assembly of the Caulobacter cell division machine. Mol Microbiol. 2011;80(6):
664 1680-98. doi: 10.1111/j.1365-2958.2011.07677.

15. Meier EL, Razavi S, Inoue T, Goley ED. A novel membrane anchor for FtsZ is linked to cell wall hydrolysis in Caulobacter crescentus. Mol Microbiol. 2016;101(2): 265-80. doi: 10.1111/mmi.13388.

16. Christen B, Abeliuk E, Collier JM, Kalogeraki VS, Passarelli B, Coller JA, et al. The essential genome of a bacterium. Mol Syst Biol. 2011;7: 528. doi: 10.1038/msb.2011.58.

17. Buss J, Coltharp C, Huang T, Pohlmeyer C, Wang SC, Hatem C, et al. In vivo organization of the FtsZ-ring by ZapA and ZapB revealed by quantitative super-resolution microscopy. Mol Microbiol. 2013;89(6): 1099-120. doi: 10.1111/mmi.12331.

18. Thanbichler M and Shapiro L. MipZ, a spatial regulator coordinating chromosome segregation with cell division in Caulobacter. Cell. 2006;126(1): 147-62.

19. Aaron M, Charbon G, Lam H, Schwarz H, Vollmer W, Jacobs-Wagner C. The tubulin homologue FtsZ contributes to cell elongation by guiding cell wall precursor synthesis in Caulobacter crescentus. Mol Microbiol. 2007;64(4): 938-52.

20. Kuru E, Hughes HV, Brown PJ, Hall E, Tekkam S, Cava F, et al. In Situ probing of newly synthesized peptidoglycan in live bacteria with fluorescent D-amino acids. Angew Chem Int Ed Engl. 2012;51(50): 12519-23. doi: 10.1002/anie.201206749.

21. Heidrich C, Templin MF, Ursinus A, Merdanovic M, Berger J, Schwarz H, et al. Involvement of N-acetylmuramyl-L-alanine amidases in cell separation and

688 antibiotic-induced autolysis of Escherichia coli. Mol Microbiol. 2001;41(1): 167-
689 78.
690 22. Uehara T, Dinh T, Bernhardt TG. LytM-domain factors are required for daughter
691 cell separation and rapid ampicillin-induced lysis in Escherichia coli. J Bacteriol.
692 2009;191(16): 5094-107. doi: 10.1128/JB.00505-09.
693 23. Uehara T, Parzych KR, Dinh T, Bernhardt TG. Daughter cell separation is
694 controlled by cytokinetic ring-activated cell wall hydrolysis. EMBO J.
695 2010;29(8): 1412-22. doi: 10.1038/emboj.2010.36.
696 24. Nierman WC, Feldblyum TV, Laub MT, Paulsen IT, Nelson KE, Eisen JA, et al.
697 Complete genome sequence of Caulobacter crescentus. Proc Natl Acad Sci USA.
698 2001;98(7): 4136-41.
699 25. Moll A, Schlimpert S, Briegel A, Jensen GJ, Thanbichler M. DipM, a new factor
700 required for peptidoglycan remodeling during cell division in Caulobacter
701 crescentus. Mol Microbiol. 2010;77(1): 90-107. doi: 10.1111/j.1365-
702 2958.2010.07224.
703 26. Goley ED, Comolli LR, Fero KE, Downing KH, Shapiro L. DipM links
704 peptidoglycan remodeling to outer membrane organization in Caulobacter. Mol
705 Microbiol. 2010;77(1): 56-73. doi: 10.1111/j.1365-2958.2010.07222.
706 27. Pogglio S, Takacs CN, Vollmer W, Jacobs-Wagner C. A protein critical for cell
707 constriction in the Gram-negative bacterium Caulobacter crescentus localizes at
708 the division site through its peptidoglycan-binding LysM domains. Mol
709 Microbiol. 2010;77(1): 74-89. doi: 10.1111/j.1365-2958.2010.07223.

710 28. Janakiraman B, Mignolet J, Narayanan S, Viollier PH, Radhakrishnan SK. In-
711 phase oscillation of global regulons is orchestrated by a pole-specific organizer.
712 Proc Natl Acad Sci USA. 2016;113(44): 12550-12555.
713 29. Radhakrishnan SK, Thanbichler M, Viollier PH. The dynamic interplay between a
714 cell fate determinant and a lysozyme homolog drives the asymmetric division
715 cycle of Caulobacter crescentus. Genes Dev. 2008;22(2): 212-25. doi:
716 10.1101/gad.1601808.
717 30. Zhou R, Chen S, Recsei P. A dye release assay for determination of lysostaphin
718 activity. Anal Biochem. 1988;171(1): 141-4.
719 31. Judd EM, Comolli LR, Chen JC, Downing KH, Moerner WE, McAdams HH.
720 Distinct constrictive processes, separated in time and space, divide Caulobacter
721 inner and outer membranes. J Bacteriol. 2005;187(20): 6874-82.
722 32. Wagner JK and Brun YV. Out on a limb: how the Caulobacter stalk can boost the
723 study of bacterial cell shape. Mol Microbiol. 2007;64(1): 28-33.
724 33. Schlimpert S, Klein EA, Briegel A, Hughes V, Kahnt J, Bolte K, et al. General
725 protein diffusion barriers create compartments within bacterial cells. Cell.
726 2012;151(6): 1270-82. doi: 10.1016/j.cell.2012.10.046.
727 34. Hughes HV, Huitema E, Pritchard S, Keiler KC, Brun YV, Viollier PH. Protein
728 localization and dynamics within a bacterial organelle. Proc Natl Acad Sci USA.
729 2010;107(12): 5599-604. doi: 10.1073/pnas.0909119107.
730 35. Kuhn J, Briegel A, Morschel E, Kahnt J, Leser K, Wick S, et al. Bactofilins, a
731 ubiquitous class of cytoskeletal proteins mediating polar localization of a cell wall

732 synthase in Caulobacter crescentus. EMBO J. 2010;29(2): 327-39. doi:
733 10.1038/emboj.2009.358.
734 36. Hughes HV, Lisher JP, Hardy GG, Kysela DT, Arnold RJ, Giedroc DP, et al. Co-
735 ordinate synthesis and protein localization in a bacterial organelle by the action of
736 a penicillin binding-protein. Mol Microbiol. 2013;90(6): 1162-77. doi:
737 10.1111/mmi.12422.
738 37. Poindexter JS and Hagenzieker JG. Novel peptidoglycans in Caulobacter and
739 Asticcacaulis spp. J Bacteriol. 1982;150(1): 332-47.
740 38. Schmidt JM and Stanier RY. The development of cellular stalks in bacteria. J Cell
741 Biol. 1966;28(3): 423-36.
742 39. Cserti E, Rosskopf S, Chang YW, Eisheuer S, Selter L, Shi J, et al. Dynamics of
743 the peptidoglycan biosynthetic machinery in the stalked budding bacterium
744 *Hyphomonas neptunium*. Mol Microbiol. 2016;103(5): 875-895. doi:
745 10.1111/mmi.13593.
746 40. Whittenbury R and Dow CS. Morphogenesis and differentiation in
747 Rhodomicrobium vannielii and other budding and prosthecate bacteria. Bacteriol
748 Rev. 1977;41(3): 754-808.
749 41. Wagner JK, Galvani CD, Brun YV. Caulobacter crescentus requires RodA and
750 MreB for stalk synthesis and prevention of ectopic pole formation. J Bacteriol.
751 2005;187(2): 544-53.
752 42. Sundararajan K, Miguel A, Desmarais SM, Meier EL, Casey Huang K, Goley ED.
753 The bacterial tubulin FtsZ requires its intrinsically disordered linker to direct

754 robust cell wall construction. Nat Commun. 2015;6: 7281. doi:
755 10.1038/ncomms8281.
756 43. Sliusarenko O, Heinritz J, Emonet T, Jacobs-Wagner C. High-throughput,
757 subpixel precision analysis of bacterial morphogenesis and intracellular spatio-
758 temporal dynamics. Mol Microbiol. 2011;80(3): 612-27. doi: 10.1111/j.1365-
759 2958.2011.07579.
760 44. Tivol WF, Briegel A, Jensen GJ. An improved cryogen for plunge freezing.
761 Microsc Microanal. 2008;14: 375-9.
762 45. Zheng SQ, Keszthelyi B, Branlund E, Lyle JM, Braunfeld MB, Sedat JW, et al.
763 UCSF tomography: an integrated software suite for real-time electron
764 microscopic tomographic data collection, alignment, and reconstruction. J Struct
765 Biol. 2007;157: 138-47.
766 46. Kremer JR, Mastronarde DN, McIntosh JR. Computer visualization of three-
767 dimensional image data using IMOD. J Struct Biol. 1996;116: 71-6.
768
769
770
771
772
773
774
775
776

Figure captions

Fig 1. Transmission electron microscopy (TEM) of chained Δ*ftsE* cells with thin, extended connections between cell bodies.

(A) Micrograph of WT cells. (B) Micrographs of Δ*ftsE* cells. * = stalk; # = skinny connection. Scale bar = 2 um.

Fig 2. *ftsE* has synthetic growth, cell length, and Z-ring structural defects with Z-ring regulator *zapA*.

(A) Phase contrast micrographs of Δ*ftsE*, Δ*zapA*, and Δ*ftsE*Δ*zapA* cells. (B) Growth curves of strains in (A). Doubling time (h) ± SEM: EG1080 = 1.78 ± 0.01; EG1133 = 1.81 ± 0.02; EG1745 = 1.86 ± 0.02. Differences between strain doubling times were ns by one-way ANOVA. (C) Cell length analyses of strains in (A). Mean cell length (μm) ± SEM: EG1080 = 2.54 ± 0.03; EG1133 = 3.50 ± 0.11; EG1745 = 3.94 ± 0.10. All pairwise comparisons of mean cell lengths yielded p values < 0.01 by one-way ANOVA. (D) FtsZ-CFP localization after 1 h of induction in WT, Δ*ftsE*, Δ*zapA*, and Δ*ftsE*Δ*zapA* cells. # = focused Z-ring; * = diffuse, punctate Z-ring. Scale bars = 2 μm.

Fig 3. Overproducing FtsE or FtsEX causes filamentation and affects the localization of FtsZ and new PG.

(A) FtsZ-CFP localization after 1 h of induction in cells bearing an empty vector (EV) or overexpressing *ftsE* or *ftsEX* for 4 h. (B) MipZ-YFP localization in cells bearing and EV or overexpressing *ftsE* or *ftsEX* for 4 h. (C) HADA labeling of cells depleted for FtsZ for

799 4 h, bearing an EV, or overexpressing *ftsE* or *ftsEX* for 4 h. * = ectopic poles. Scale bars
800 = 2 μm.
801
802 **Fig 4**. Synthetic genetic interactions between *amiC*, *ftsE*, and *ldpF*.
803 Phase contrast micrographs and serial spot dilutions of (A) WT, Δ*ftsE*, and Δ*ldpF*; (B)
804 WT and Δ*ftsE* cells depleted for AmiC for 24 h; (C) WT and Δ*ldpF* cells depleted for
805 AmiC for 24 h; (D) WT and Δ*ldpF* cells depleted for FtsE for 24 h. Scale bar = 2 μm.
806
807 **Fig 5**. Synthetic genetic interactions between *dipM* and *amiC*, *ftsE*, or *ldpF* and between
808 *ftsE* and *spmX*.
809 Phase contrast micrographs and serial spot dilutions of (A) WT, Δ*ftsE*, and Δ*dipM*; (B)
810 WT and Δ*dipM* cells depleted for AmiC for 24 h; (C) WT and Δ*ftsE* cells depleted for
811 DipM for 24 h; (D) WT and Δ*ldpF* cells depleted for DipM for 24 h; (E) Δ*spmX* and
812 Δ*ftsE*Δ*spmX*. Scale bar = 2 μm.
813
814 **Fig 6**. Electron cryotomography (ECT) of cells lacking FtsE and AmiC reveal stalk-like
815 connections between cell bodies.
816 (A) WT *C. crescentus* stalk with cross-bands. (B) *ftsE* mutants with skinny connections
817 most similar to stalks. (C) *ftsE* mutants with skinny connections that are stalk-like, but
818 that have regions with heterogeneous widths. (D) *ftsE* mutants with skinny connections
819 that are fairly short with inner membranes that are close together or nearly fused.
820 Abbreviations are as follows: OM = outer membrane, PG = peptidoglycan, IM = inner

821 membrane. # = cross-band; * = cross-band-like structure. Scale bar (A) = 200 nm; Scale
822 bars (B-D) = 100 nm.
823
824 **Fig 7**. Stalk specific proteins StpX and PbpC localize to the skinny constrictions in *ftsE*
825 mutants.
826 (A) Localization of StpX-CFP induced for 18 h in WT, Δ*ftsE* or Δ*ftsE* cells depleted for
827 AmiC for 18 h. (B) Localization of StpX-CFP induced for 2.75 h in Δ*ftsE*Δ*pbpC*. (C)
828 Localization of Venus-PbpC induced for 2 h in WT or Δ*ftsE*. (D) Localization of cross-
829 band protein StpB-mCherry induced for 18 h in WT, Δ*ftsE* or Δ*ftsE* cells depleted for
830 AmiC for 18 h. # = stalk enrichment; * = skinny connection enrichment. Scale bars = 2
831 μm.
832
833 **Fig 8**.
834 FtsEX-mediated regulation of constriction initiation and final cell separation reveals
835 morphogenetic plasticity in *C. crescentus*.
836 (A) Cell cycle localization of FtsZ and stalk proteins in WT and Δ*ftsE* cells. (B) Three
837 putative cell separation pathways in *C. crescentus*.
838

839 **Supporting Information Captions**

840 **Fig S1**. *In vivo* LdpF-mCherry has a diffuse, patchy localization in WT and Δ*ftsE*.

841 (A) Predicted domain organization of *E. coli* EnvC and *C. crescentus* LdpF. (B)

842 Localization of LdpF-mCherry induced for 4 h in WT or Δ*ftsE*. Abbreviations are as

843 follows: SS = signal sequence; CC = coiled coil domain; LytM = LytM domain. Scale bar

844 = 2 μm.

845

846 **Fig S2**. LdpF binds the extracellular loop (ECL) of FtsX but does not activate AmiC *in*

847 *vitro*.

848 (A) Bacterial two-hybrid of T18 and T25 fusions to the ECL of FtsX, the coiled coil

849 domain (CC) of LdpF, and the CC cytoplasmic protein ZauP, which was used as a

850 negative control. (B,C) Dye release assay with RBB-labeled sacculi and purified variants

851 of AmiC, LdpF, DipM, and the ECL of FtsX. Each protein was used at 4 μM and

852 reactions were incubated at 30^{o}C for 3 h. Reactions were performed in triplicate. *** =

853 $p < 0.0001$ by one-way ANOVA.

854

855 **Fig S3**. Electron cryotomography (ECT) of cells lacking FtsE and AmiC reveal stalk-like

856 connections of heterogeneous widths.

857 (A) *ftsE* mutant with skinny connections that are stalk-like, but have regions with

858 heterogeneous widths. (B) WT *C. crescentus* stalks with cross-bands. # = cross-band.

859 Scale bar (A) = 100 nm; Scale bars (B) = 200 nm.

860

861 **Fig S4**. *ftsE* mutants incorporate new cell wall material throughout skinny connections
862 between cell bodies.
863 HADA labeling of (A) WT, (B) Δ*ftsE*, and (C) Δ*ftsE* cells depleted for AmiC for 6 h. (D)
864 FtsZ-CFP localization after 1 h of induction in Δ*ftsE* cells. * = HADA incorporation
865 throughout skinny connections in Δ*ftsE*; # = absence of FtsZ at skinny connections in
866 Δ*ftsE*. Scale bars = 2 μm.
867
868 **Fig S5**. Overproducing LdpF, the LytM domain (LytM) of LdpF or AmiC is not lytic *in*
869 *vivo*.
870 Phase contrast images of cells overproducing LdpF, the LytM of LdpF or AmiC for 24 h.
871 Scale bar = 2 μm.
872
873 **Text S1.** Supporting results and discussion describing biochemical investigation of cell
874 wall hydrolase activities of LytM proteins and AmiC.
875
876 **Table S1.** Strains and plasmids used in this study with their methods of construction.

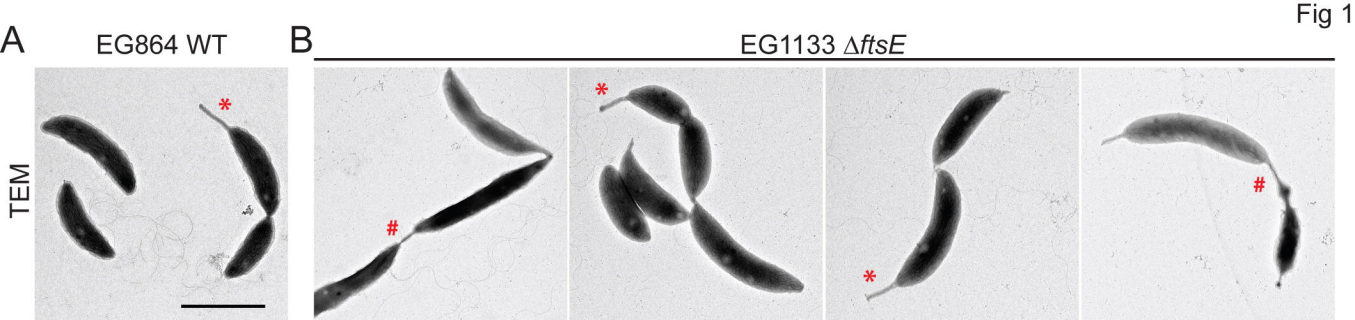
A
EG864 WT
B
EG1133 ΔftsE
TEM
*
#
*
*
#

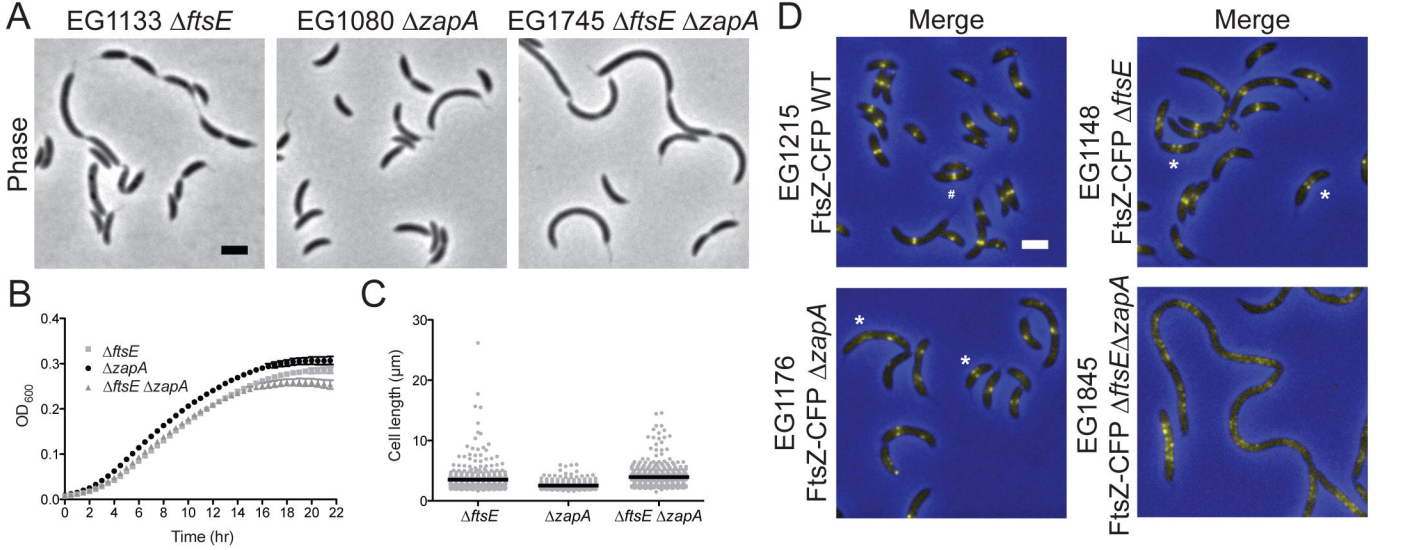
A
EG1133 ΔftsE
EG1080 ΔzapA
EG1745 ΔftsE ΔzapA
Phase
B
ΔftsE
ΔzapA
ΔftsE ΔzapA
OD600
Time (hr)
C
Cell length (μm)
ΔftsE
ΔzapA
ΔftsE ΔzapA
D
Merge
Merge
EG1215
FtsZ-CFP WT
EG1148
FtsZ-CFP ΔftsE
EG1176
FtsZ-CFP ΔzapA
EG1845
FtsZ-CFP ΔftsEΔzapA

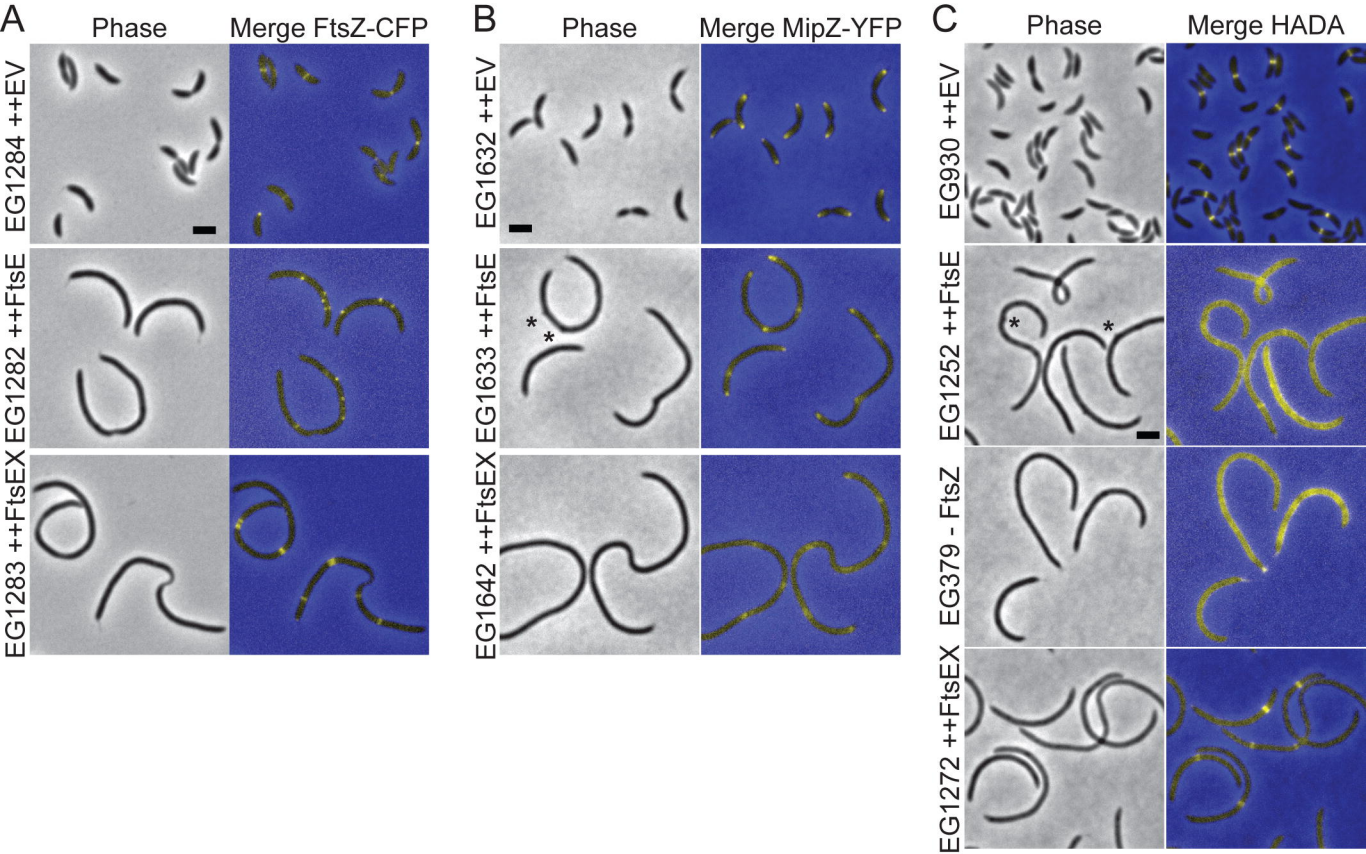
A
Phase
Merge FtsZ-CFP
EG1284 ++EV
EG1282 ++FtsE
EG1283 ++FtsEX
B
Phase
Merge MipZ-YFP
EG1632 ++EV
EG1633 ++FtsE
EG1642 ++FtsEX
C
Phase
Merge HADA
EG930 ++EV
EG1252 ++FtsE
EG379 - FtsZ
EG1272 ++FtsEX

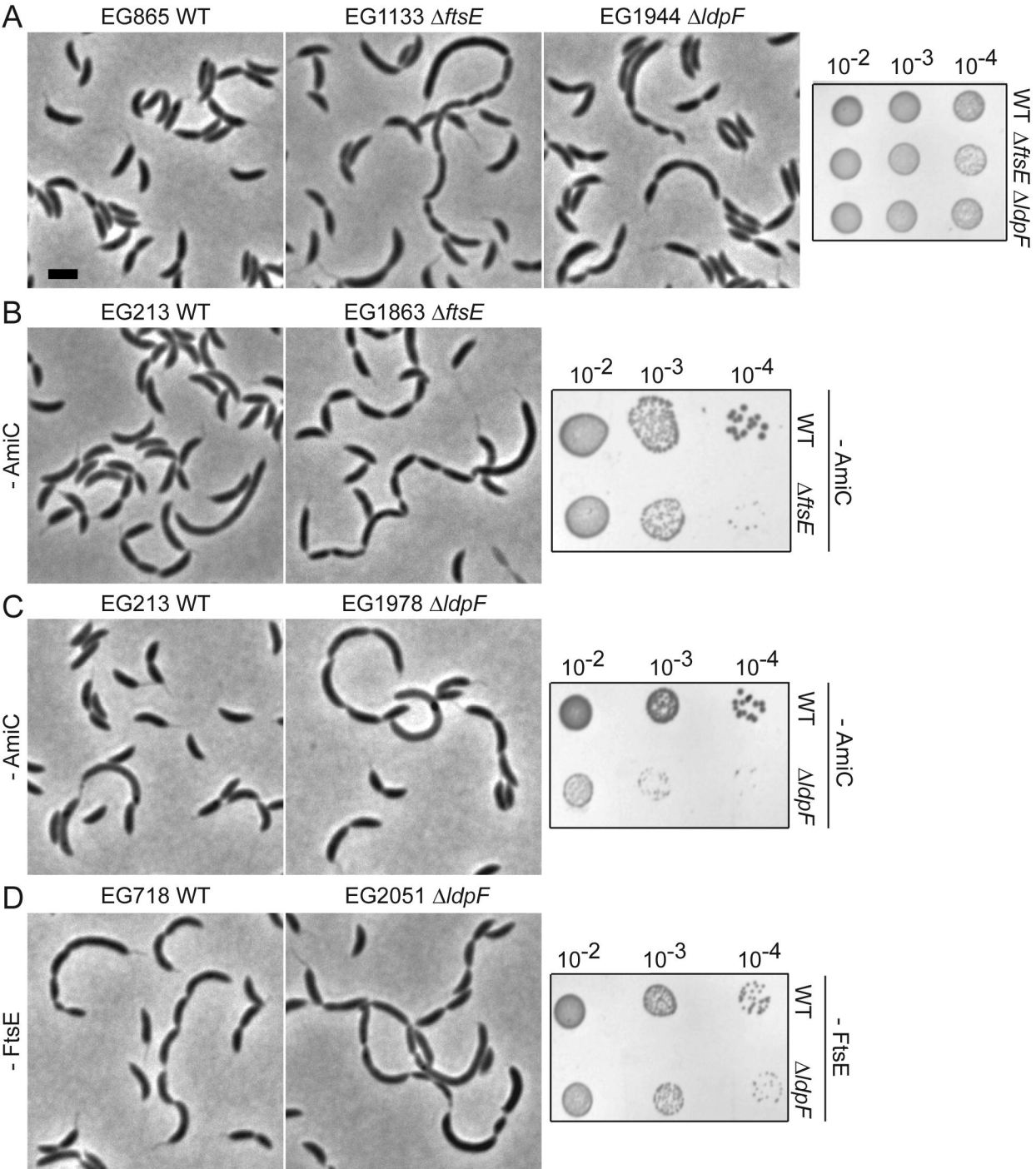
A
EG865 WT
EG1133 ΔftsE
EG1944 ΔldpF
10-2
10-3
10-4
WT
ΔftsE
ΔldpF
B
EG213 WT
EG1863 ΔftsE
- AmiC
10-2
10-3
10-4
WT
ΔftsE
- AmiC
C
EG213 WT
EG1978 ΔldpF
- AmiC
10-2
10-3
10-4
WT
ΔldpF
- AmiC
D
EG718 WT
EG2051 ΔldpF
- FtsE
10-2
10-3
10-4
WT
ΔldpF
- FtsE

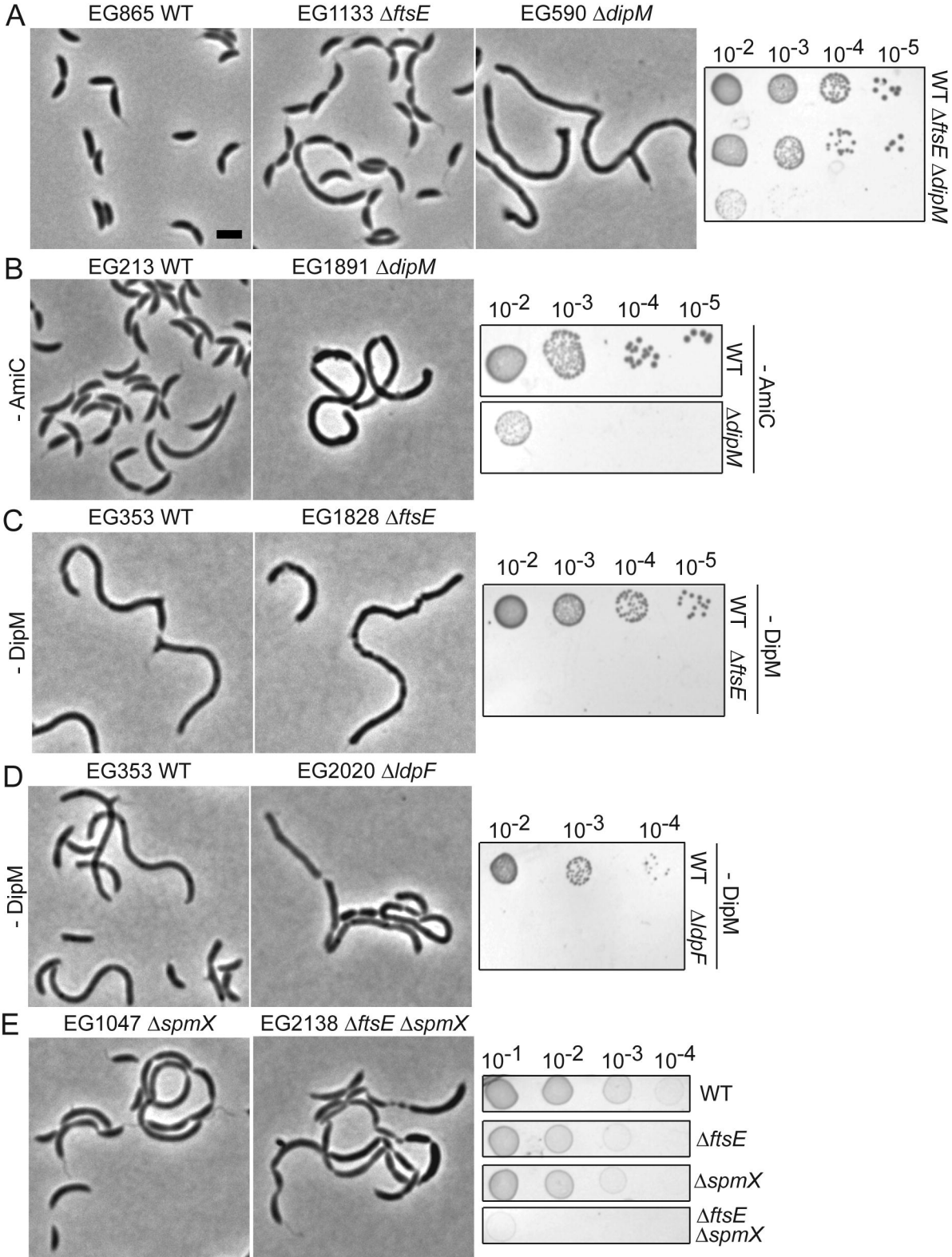
A
EG865 WT
EG1133 ΔftsE
EG590 ΔdipM
10-2 10-3 10-4 10-5
WT ΔftsE ΔdipM
B
EG213 WT
EG1891 ΔdipM
- AmiC
10-2 10-3 10-4 10-5
WT
ΔdipM
- AmiC
C
EG353 WT
EG1828 ΔftsE
- DipM
10-2 10-3 10-4 10-5
WT
ΔftsE
- DipM
D
EG353 WT
EG2020 ΔldpF
- DipM
10-2 10-3 10-4
WT
ΔldpF
- DipM
E
EG1047 ΔspmX
EG2138 ΔftsE ΔspmX
10-1 10-2 10-3 10-4
WT
ΔftsE
ΔspmX
ΔftsE
ΔspmX

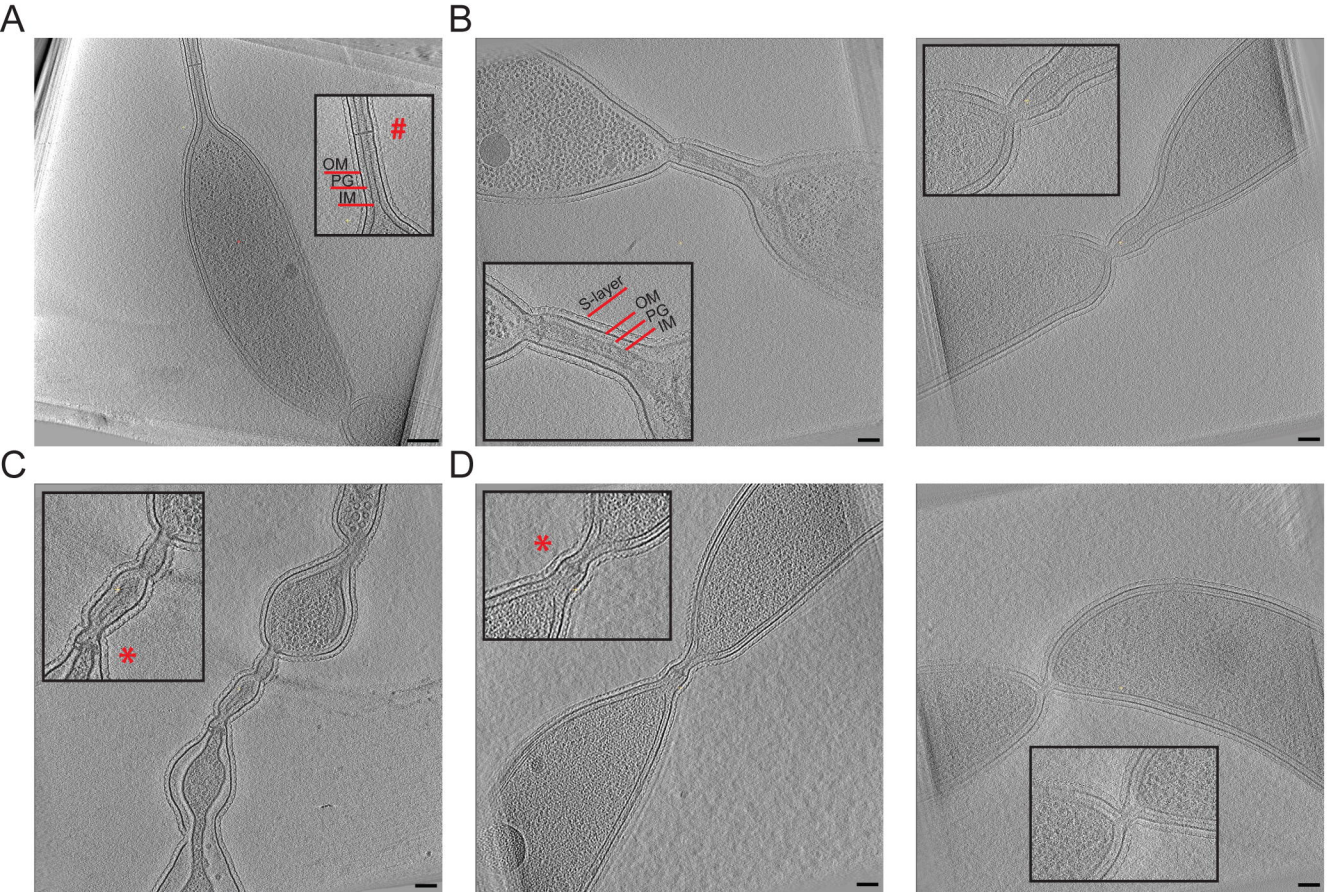
A
#
OM
PG
IM
B
S-layer
OM
PG
IM
C
*
D
*

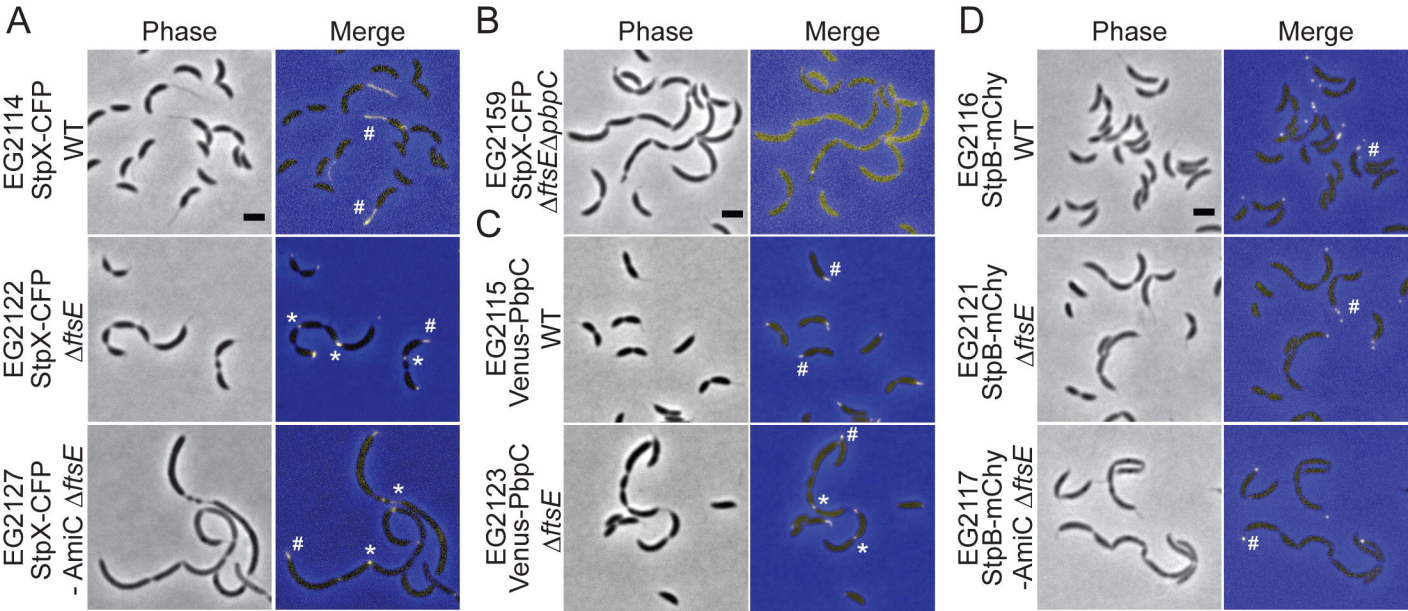
A
Phase
Merge
EG2114
StpX-CFP
WT
EG2122
StpX-CFP
ΔftsE
EG2127
StpX-CFP
- AmiC ΔftsE
B
EG2159
StpX-CFP
ΔftsEΔpbpC
C
EG2115
Venus-PbpC
WT
EG2123
Venus-PbpC
ΔftsE
D
EG2116
StpB-mChy
WT
EG2121
StpB-mChy
ΔftsE
EG2117
StpB-mChy
-AmiC ΔftsE

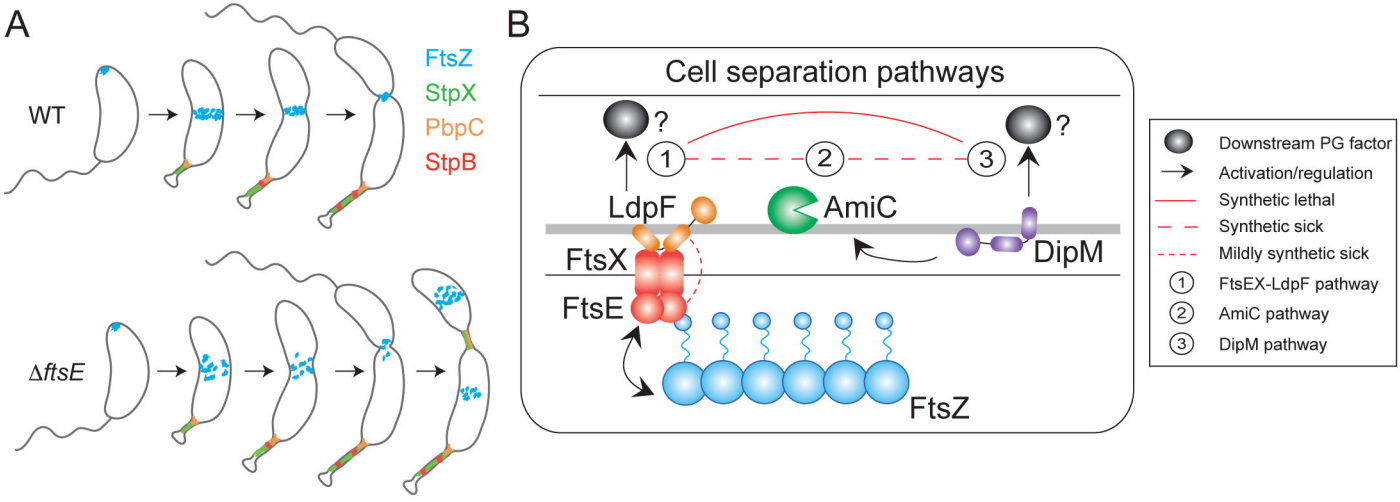
A
WT
ΔftsE
FtsZ
StpX
PbpC
StpB
B
Cell separation pathways
?
?
1
2
3
LdpF
AmiC
DipM
FtsX
FtsE
FtsZ
Downstream PG factor
Activation/regulation
Synthetic lethal
Synthetic sick
Mildly synthetic sick
1 FtsEX-LdpF pathway
2 AmiC pathway
3 DipM pathway